

improved Saturation Performance in High Speed Waveguide Photodetectors at 1.3  $\mu\text{m}$   
using an asymmetric InAlGaAs/InGaAsP structure

T. A. Vang, L. Davis, S. Keo and S. F. Forouhar

Jet Propulsion Laboratory  
4800 Oak Grove Drive  
Pasadena, CA 91109

ABSTRACT

Improved saturation and linearity characteristics are realized in waveguide p-i-n photodetectors at 1.3  $\mu\text{m}$  by using an asymmetric cladding structure with InAlGaAs in the anode and InGaAsP in the cathode. Multi-mode structures show efficiencies of 0.61, DC photocurrent saturation of more than 8.5 mA and an RC limited bandwidth of 13 GHz. The -60dBc point of the first harmonic is at a photocurrent of 3.6 mA with a bias of -3 V. A comparison is made to a symmetric InGaAsP/InP waveguide structure, with the asymmetric structure showing roughly a factor of 2 improvement in both the saturation and harmonic distortion at high input powers.

I. INTRODUCTION

Waveguide photodetector (WGPDS) results have recently been presented [1]-[3] demonstrating the very large bandwidth-efficiency product potential of these devices. The advantage of using a waveguide geometry as a photodetector comes from the decoupling of the transit-time limited frequency response and the quantum efficiency by having the photocurrent flow perpendicularly to the optical transmission [4]. Bandwidths of 176 GHz and bandwidth-efficiency products as high as  $\sim 6$  GHz have been reported in GaAs/AlGaAs WGPDS [2]. Similarly, bandwidths of 110 GHz and bandwidth-efficiency products up to 55 GHz have been demonstrated in InGaAs/InP based WGPDS [3]. These results illustrate the advantages of WGPDS over normally incident photodetectors which have a bandwidth-efficiency product limit of around 25 GHz [4]. Improvements in the bandwidths of WGPDS have come through reducing the RC limits [3], and by using a traveling wave WGPDS geometry that replaces the RC limit with a velocity mismatch limitation providing even greater bandwidths [2]. The efficiency of WGPDS is essentially determined by the incident coupling efficiency, and here again a number of improvements have been realized

using multi-transverse mode layer structures [5]. It is also possible to integrated passive mode converters [6] to increase the coupling efficiency.

The large bandwidth-efficiency product of these detectors makes them attractive for a number of applications, including RF optical links. In this case, the linearity and saturation of the detector is also of great importance, as in an externally modulated RF link the noise figure and the insertion loss can be reduced by increasing the optical power transmitted through the link [7]. These optical links are primarily of interest at 1.3  $\mu\text{m}$  and 1.55  $\mu\text{m}$  wavelengths due to optical fiber transmission characteristics, and many of the desired RF carrier frequencies are beyond 25 GHz. These wavelength and bandwidth requirements lead to the need for high speed and high saturation power InP-based WGPDS. The saturation effect of WGPDS has drawn both theoretical interest [8] and some experimental results [9- 10]. In this letter we report on the bandwidth, efficiency and saturation effects of two WGPDS designs including a standard InGaAs/InGaAsP/InP structure and a novel InGaAs/InAlGaAs/InGaAsP/InP structure that offers improved saturation performance.

## II. DESIGN AND FABRICATION

The two WGPDS structures presented here were grown on semi-insulating Fe-doped InP substrates by low pressure metal organic vapor phase epitaxy using Zn and Si as the  $p$  and  $n$  type dopants respectively. As shown in Fig. 1, the WGPDS are ridge structures that were fabricated using metal lift-offs and wet chemical etching. Ti/Pt/Au is used for  $p$ -contact metalization and for the self-aligned ridge etch. AuGe/Ni/Au is used for the  $n$ -contact metal and photoresist is used as a mask for the etch to the semi-insulating InP substrate. Polyimide is used for planarization and passivation. Vias in the polyimide are dry etched using  $\text{O}_2$  RIE to expose both the  $p$  and  $n$  metals, and Ti/Au coplanar waveguide (CPW) pads are formed for final contacts. The samples were then lapped to  $\sim 100$   $\mu\text{m}$  followed by Ti/Au back side metalization for mounting. Bars were cleaved to  $\sim 400$   $\mu\text{m}$  length which yielded  $\sim 25$   $\mu\text{m}$  long WGPDS. Ridge widths of 4  $\mu\text{m}$ , 7  $\mu\text{m}$ , 10  $\mu\text{m}$  and 13

$\mu\text{m}$  were formed, all of which are multi-mode in the lateral direction. Fig. 2 shows the two layer structures used for comparison. Structure 1 has lattice matched InGaAsP ( $\lambda_{\text{PL}} = 1.18 \mu\text{m}$ ) adjacent to both sides of the absorbing region followed by InP cladding layers. Structure 2 has InP and InGaAsP on the n-side of the InGaAs, but it has lattice matched InAlGaAs and InAlAs on the p-side of the InGaAs. The InAlGaAs is graded from  $\lambda_{\text{PL}} = 1.13 \mu\text{m}$  to  $\lambda_{\text{PL}} = 0.95 \mu\text{m}$  before the  $1.0 \mu\text{m}$  of InAlAs is grown. Both structures have  $6000 \text{ \AA}$  intrinsic regions which yield transit time limited bandwidths of  $\sim 49 \text{ GHz}$  [5]. Structure 1 was designed as a baseline structure to make comparisons to previous work. In the vertical direction (perpendicular to the junction) it has both the fundamental and first order waveguide modes. Structure 2 was designed to also include the second order mode, which can have a significant modal overlap with the incident mode from the fiber. This results in an improved coupling efficiency. The use of the InAlGaAs and InAlAs in structure 2 reduces the valence band offset for photogenerated holes on the p-side of the intrinsic region. This will increase the thermionic emission process and reduce the carrier induced screening effects attributed to saturation in the detector [8]. The use of an all InAlGaAs/InAlAs WGPD has been reported [11], but here we see improved performance by retaining the InGaAsP/InP on the n-side of the device to maintain the smaller conduction band offset for the photogenerated electrons.

### III. DEVICE CHARACTERISTICS

A number of devices from both structures were measured for dark current, breakdown voltage, capacitance and series resistance. Typical results are summarized in Table 1. The series resistance of both structures is likely dominated by the specific contact resistance of the p-contact, and for simplicity we lump the measured forward differential resistance into this value. The dark current, breakdown voltage, capacitance and series resistance are all somewhat worse for structure 2, and this can be attributed to the presence of InAlGaAs and

InAlAs in the etched ridge region. The increased leakage current was dominated by a surface effect, as it could be dramatically reduced when measured immediately after a brief etch in dilute HF. Thus, we hope to improve the leakage current by better surface passivation. The lower breakdown voltage of structure 2 seems to be a bulk effect as it was not significantly affected by the dilute HF etch. The larger capacitance of structure 2 is due to the isotropic wet etching used to define the ridge. This is a timed etch which leaves a small amount of InAlGaAs exposed outside of the ridge, effectively increasing the diode area. This will likely contribute to the larger leakage current and may also affect the breakdown voltage. Here a dry etching process will equalize the areal capacitances of the two structures and may improve the leakage current and breakdown voltage. The series resistance of both structures will limit the bandwidth well below the transit time limit. Use of an alloyed p-contact such as AuZn is expected to reduce the specific contact resistance by a factor of 10 or more. This will enable  $7\ \mu\text{m} \times 14\ \mu\text{m}$  ( $\sim 100\ \mu\text{m}^2$ ) devices to match the 49 GHz transit time limited bandwidth, while still providing more than 99.9% absorption of the guided light.

Fig. 3 shows the DC optical power saturation measurements for both structures with device areas of  $7\ \mu\text{m} \times 25\ \mu\text{m}$ . The measurements were made using a diode-pumped Nd:YAG laser, a calibrated optical attenuator, and a hemispherically lensed fiber with a radius of  $\sim 10\ \mu\text{m}$ . The responsivity of the devices from structures 1 and 2 are  $0.36\ \text{A/W}$  and  $0.65\ \text{A/W}$ , yielding efficiencies of  $\sim 0.34$  and  $\sim 0.61$ , respectively. The improvement for the InAlGaAs device results from improved optical coupling efficiency which is due to a single layer  $\text{AlO}_x$  coating, the addition of the second order transverse mode and the narrower ridge. The reflectivity of the  $\text{AlO}_x$  coating is estimated to be  $\sim 8\%$ , and the additional transverse mode and narrower ridge both lead to a better modal overlap with the incident light. We did not compare  $4\ \mu\text{m}$  ridge devices as the InAlGaAs structures had very high series resistances due to the isotropic etching. A definite improvement in DC saturation can be seen for structure 2 as it maintains a linear response beyond  $8.5\ \text{mA}$  of photocurrent, whereas

structure 1 shows some saturation effects near 3.5 mA. The limit on the measured photocurrent for structure 2 was due to the maximum calibrated laser output and the insertion loss of the attenuator (approximately 3 dB). The responsivity of structure 2 without the attenuator (full laser power) was  $-0.55$  A/W indicating some saturation was occurring between 8.5 mA and 17.0 mA.

Fig. 4 shows the harmonic response of each structure versus average photocurrent (optical power) at a  $-3$  V bias. The bias was applied using a Keithley 237 source-measure unit and a 0.1 - 18 GHz bias tee. Contact to the devices was made using a 40 GHz CPW probe, and the harmonics were measured on an HP 5692A spectrum analyzer using two Nd:YAG lasers matched in power with a fundamental beat frequency of 500 MHz. The two lasers were free running which limited the noise floor to  $-70$  dBm. Also shown in Fig. 4 are the  $-60$  dBc points, which are at approximately 1.8 mA and 3.6 mA for structures 1 and 2, respectively. This shows that the InAlGaAs structure has better linearity performance than the standard InGaAsP structure at high optical powers. In both structures RF compression can be observed at the highest input powers.

The frequency response of  $7 \mu\text{m} \times 25 \mu\text{m}$  devices from each structure were measured by piezoelectrically tuning one of the Nd:YAG lasers and again measuring the microwave power on an HP 5962A spectrum analyzer. Fig. 5 shows the uncorrected frequency response of the two structures. The ripple in the response is due to impedance mismatch between the device and the  $50 \Omega$  CPW probe. This mismatch also results in differences in the measured microwave power for each device. The  $-3$  dB bandwidths for low optical input power are approximately 18 GHz and 13 GHz, for structures 1 and 2 respectively. These are in reasonable agreement with the RC limits of each device. In structure 1 the roll-off of the response is not significantly affected by the increase in optical power up to the maximum photocurrent of 4.6 mA. Similarly, in structure 2 the response at 4.6 mA is relatively unaffected; however, there is evidence of saturation at the maximum photocurrent

of 8.5 mA. This shows that the DC saturation measurement is not necessarily a good measure of the microwave saturation of the detector.

#### IV. CONCLUSION

Previous work has demonstrated that WGPDS offer excellent performance for high frequency optical communication applications. We have demonstrated an improvement in optical saturation and linearity of InP-based WGPDS by using an asymmetric cladding structure using InGaAsP/InP on the cathode and InAlGaAs/InAlAs on the anode: DC saturation measurements show more than a factor of 2 improvement in saturation photocurrent to more than 8.5 mA for the asymmetric structure. Measurement of the harmonics also show an improvement in linearity at high powers. Frequency response measurements demonstrate RC-limited performance dominated by the p-contact resistivity. These results indicate that asymmetric WGPDS can offer improved performance for high power RF optical communication links and can be used for a variety of high power microwave source applications.

## REFERENCES

1. D. Wake, T. P. Spooner, S. D. Perrin, I. D. Henning, "50 GHz InGaAs Edge-Coupled *pin* Photodetector," *Electron. Lett.*, vol. 27, no. 12, pp. 1073-1075, 1991.
2. K. S. Giboney, R. L. Nagarajan, T. E. Reynolds, S. T. Allen, R. P. Mirin, M. J. Rodwell, and J. E. Bowers, "Travelling-Wave Photodetectors with 172-GHz Bandwidth and 76-GHz Bandwidth-Efficiency Product," *IEEE Photon. Technol. Lett.*, vol. 7, no. 4, pp. 412-414, 1995.
3. K. Kate, A. Kozen, Y. Muramoto, Y. Itaya, T. Nagatsuma, and M. Yaita, "110-GHz, 50%-efficiency mushroom-mesa waveguide p-i-n photodiode for 1.55- $\mu$ m wavelength," *IEEE Photon. Technol. Lett.*, vol. 6, no. 6, pp. 719-721, 1994.
4. J. E. Bowers and C. A. Burrus, Jr., "Ultrawide-Band Long-Wavelength p-i-n Photodetectors," *J. Lightwave Tech.*, vol. LT-5, no. 10, pp. 1339-1350, 1987.
5. K. Kate, S. Hata, K. Kawano, and A. Kozen, "Design of Ultrawide-Band, High-Sensitivity p-i-n Photodetectors," *IEICE Trans. Electron.*, vol. E76-C, no. 2, pp. 214-221, 1993.
6. R. Ben-Michael, U. Koren, B. I. Miller, M. G. Young, M. Chien, and G. Raybon, "InP-Based Multiple Quantum Well Lasers with an Integrated Tapered Beam Expander Waveguide," *IEEE Photon. Technol. Lett.*, vol. 6, no. 12, pp. 1412-1414, 1994.
7. C. H. Cox III, G. E. Betts, and L. M. Johnson, "An Analytic and Experimental Comparison of Direct and External Modulation in Analog Fiber-Optic Links," *IEEE Trans. Microwave Theory Tech.*, vol. 38, no. 5, pp. 501-509, 1990.
8. J. Harari, F. Journet, O. Rabbi, G. Jin, J. P. Vilcot, and D. Decoster, "Modeling of Waveguide PIN Photodetectors Under Very High Optical Power," *IEEE Trans. Microwave Theory Tech.*, vol. 43, no. 9, pp. 2304-2310, 1995.
9. A. R. Williams, A. L. Kellner, and P. K. L. Yu, "High Frequency Saturation Measurements of an InGaAs/InP Waveguide Photodetector," *Electron. Lett.*, vol. 29, no. 21, pp. 1879-1881, 1993.
10. D. Wake, N. G. Walker, and I. C. Smith, "Zero-Bias edge coupled InGaAs photodiodes in millimeter wave radio fiber systems," *Electron. Lett.*, vol. 29, no. 14, pp. 1298-1299, 1993.
11. G. Hasnain, C. J. Madden, V. M. Robbins, and C. Y. Su, "Fast, Efficient and Highly Linear InGaAlAs Waveguide PIN Photodetectors," *Integrated Photonics Research Meeting, Postdeadline Papers*, Santa Barbara, CA, 1994.

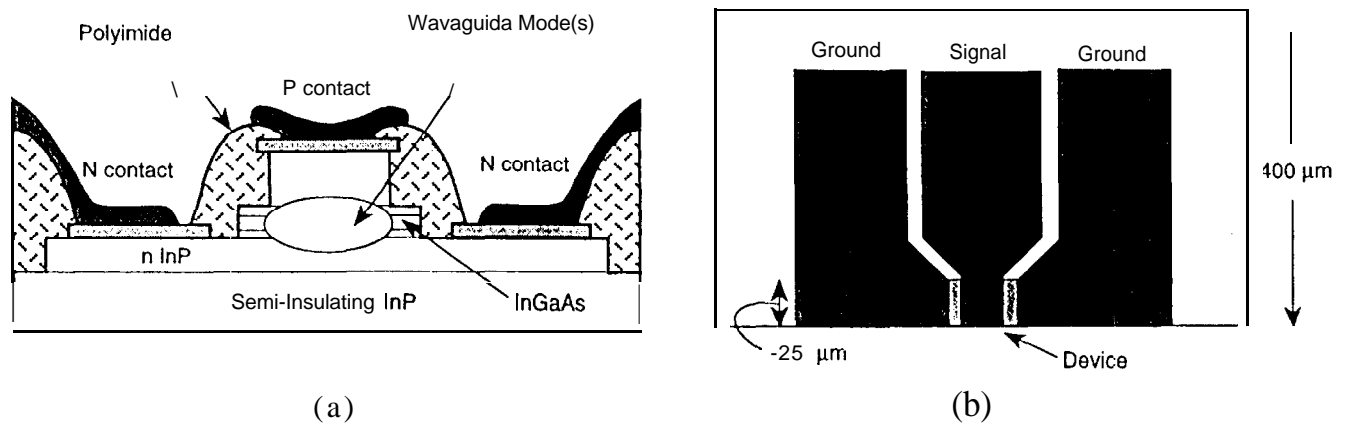


Fig. 1. (a) Schematic cross section of the incident facet of a waveguide p-i-n photodetector. Ridge widths defined by the p metal are  $4 \mu\text{m}$ ,  $7 \mu\text{m}$ ,  $10 \mu\text{m}$  and  $13 \mu\text{m}$ . (b) Schematic top view of a cleaved device showing the coplanar waveguide electrical contacts.

Structure 1

Material	Thickness	Doping
$\text{In}_{0.53}\text{Ga}_{0.47}\text{As}$	$0.1 \mu\text{m}$	p+
InP	$0.8 \mu\text{m}$	p
$\text{InGaAsP}(\lambda = 1.18\mu\text{m})$	$0.1 \mu\text{m}$	u/d
$\text{In}_{0.53}\text{Ga}_{0.47}\text{As}$	$0.4 \mu\text{m}$	u/d
$\text{InGaAsP}(\lambda = 1.18\mu\text{m})$	$0.1 \mu\text{m}$	u/d
InP	$1.0 \mu\text{m}$	n+
$\text{In}_{0.53}\text{Ga}_{0.47}\text{As}$	$0.05 \mu\text{m}$	n+
InP	substrate	SI(Fe)

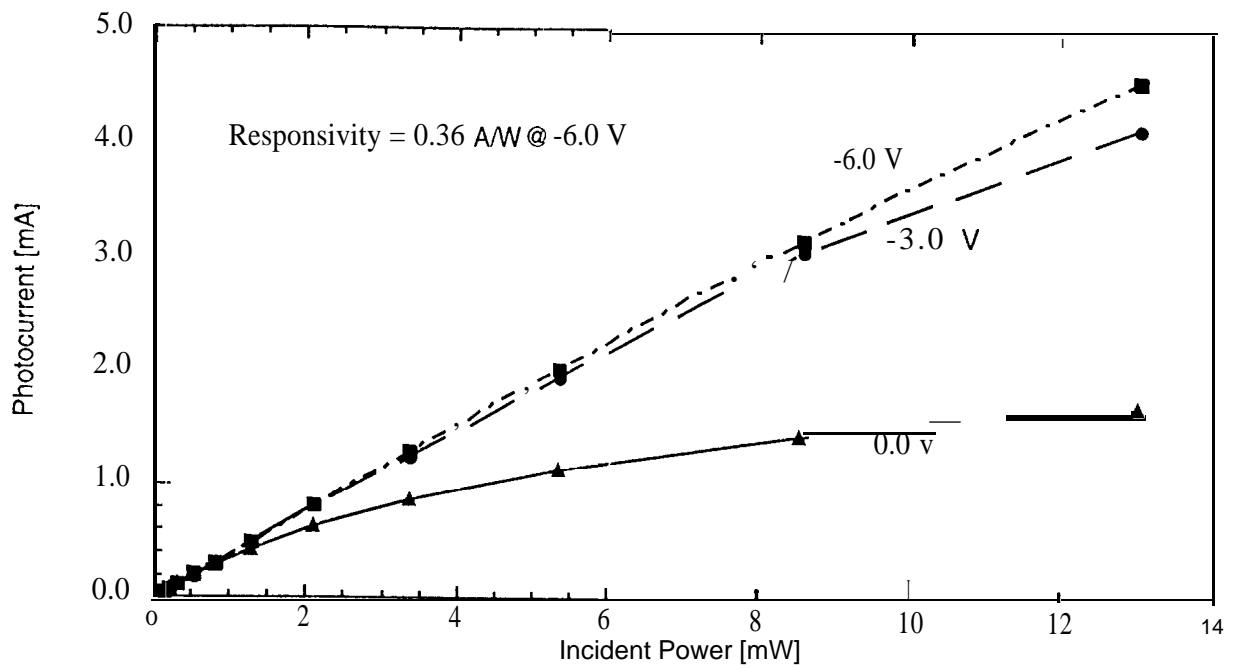
Structure 2

Material	Thickness	Doping
$\text{In}_{0.53}\text{Ga}_{0.47}\text{As}$	$0.1 \mu\text{m}$	p+
$\text{In}_{0.52}\text{Al}_{0.48}\text{As}$	$1.0 \mu\text{m}$	p
$\text{InAlGaAs}(\text{graded})$	$0.4 \mu\text{m}$	p
$\text{InAlGaAs}(\text{graded})$	$0.1 \mu\text{m}$	u/d
$\text{In}_{0.53}\text{Ga}_{0.47}\text{As}$	$0.5 \mu\text{m}$	u/d
$\text{InGaAsP}(\lambda = 1.18\mu\text{m})$	$0.25 \mu\text{m}$	n
$\text{InGaAsP}(\lambda = 1.10\mu\text{m})$	$0.5 \mu\text{m}$	n
InP	$1.0 \mu\text{m}$	n+
$\text{In}_{0.53}\text{Ga}_{0.47}\text{As}$	$0.05 \mu\text{m}$	n+
InP	substrate	SI(Fe)

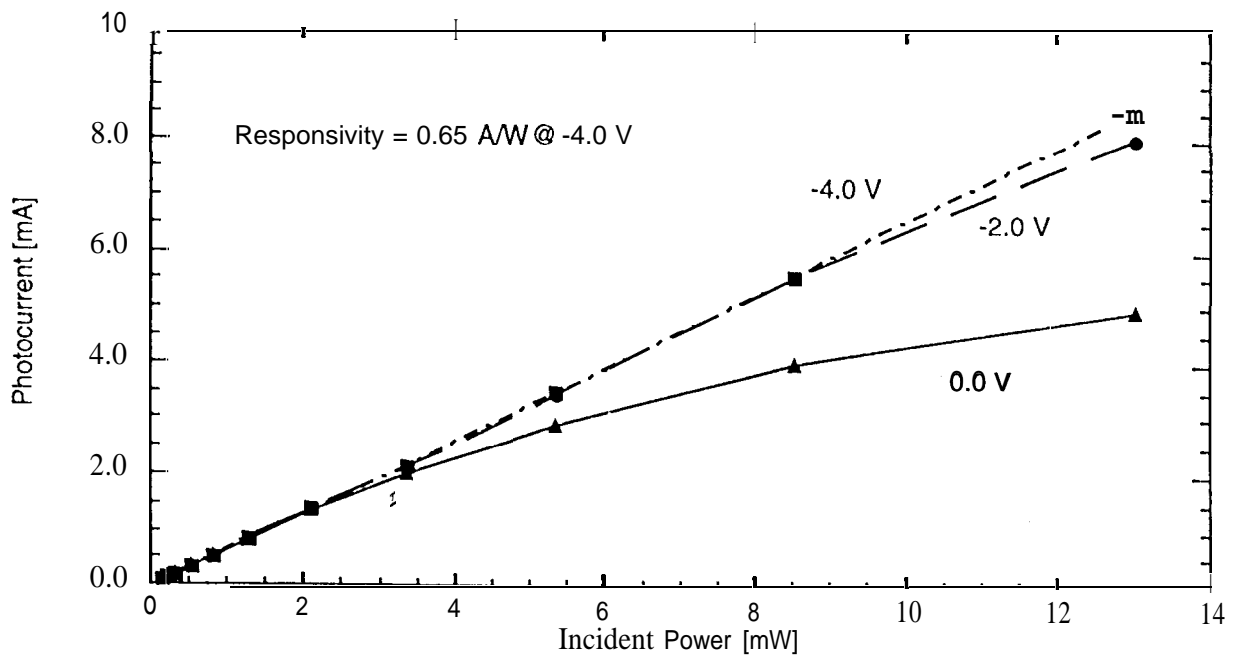
Fig. 2. Layer structures for both waveguide p-i-n photodetectors. Both structures have a  $0.6 \mu\text{m}$  intrinsic region for a transit time limited bandwidth of  $\sim 49 \text{ GHz}$ . In structure 2 the  $0.1 \mu\text{m}$  thick undoped InAlGaAs layer is graded from  $\lambda \approx 1.13 \mu\text{m}$  to  $1.10 \mu\text{m}$  and the  $0.4 \mu\text{m}$  thick p-doped InAlGaAs layer is graded from  $\lambda \approx 1.10 \mu\text{m}$  to  $0.95 \mu\text{m}$ .

TABLE 1  
Electrical Properties of the WGPD structures

Property	Structure 1	Structure 2
Dark Current Density (@ -3V)	$\leq 5.5 \text{ pA}/\mu\text{m}^2$	$\leq 35 \text{ pA}/\mu\text{m}^2$
Reverse Breakdown (@ 100nA)	-12V	-5 V
Capacitance (@1 MHz and -3 V)	$0.38 \text{ fF}/\mu\text{m}^2$	$0.50 \text{ fF}/\mu\text{m}^2$
Series Resistance (forward differential)	$1.4 \times 10^{-4} \Omega \text{ cm}^2$	$1.6 \times 10^{-4} \Omega \text{ cm}^2$

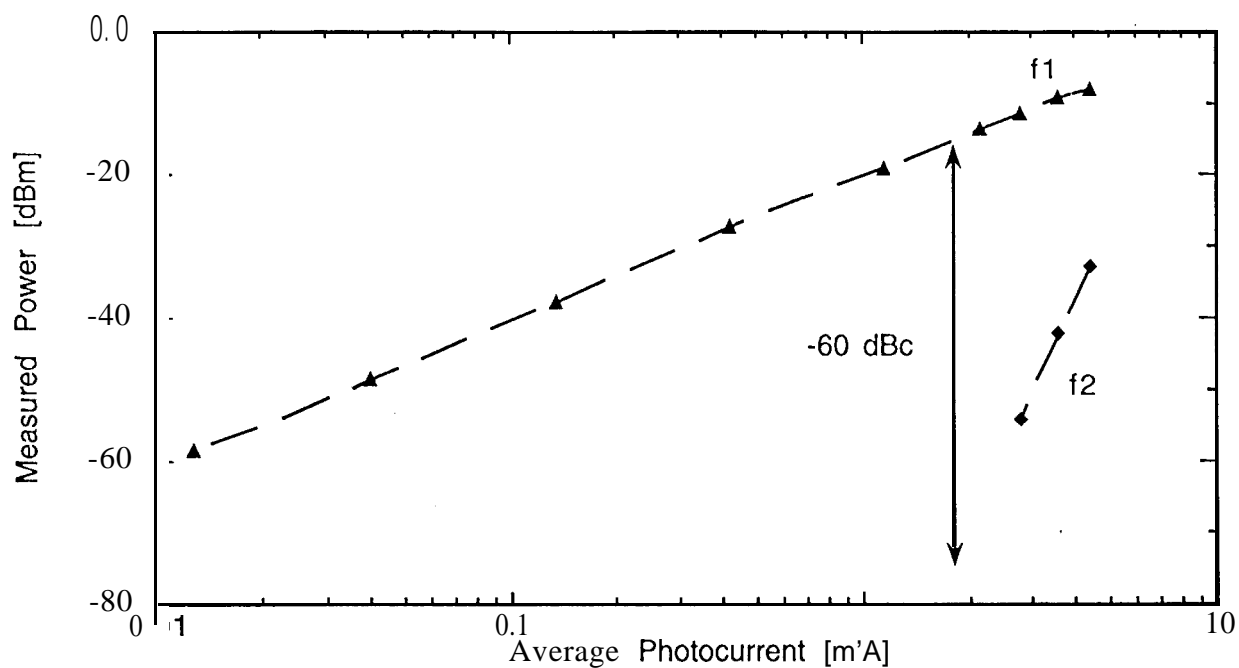


(a)

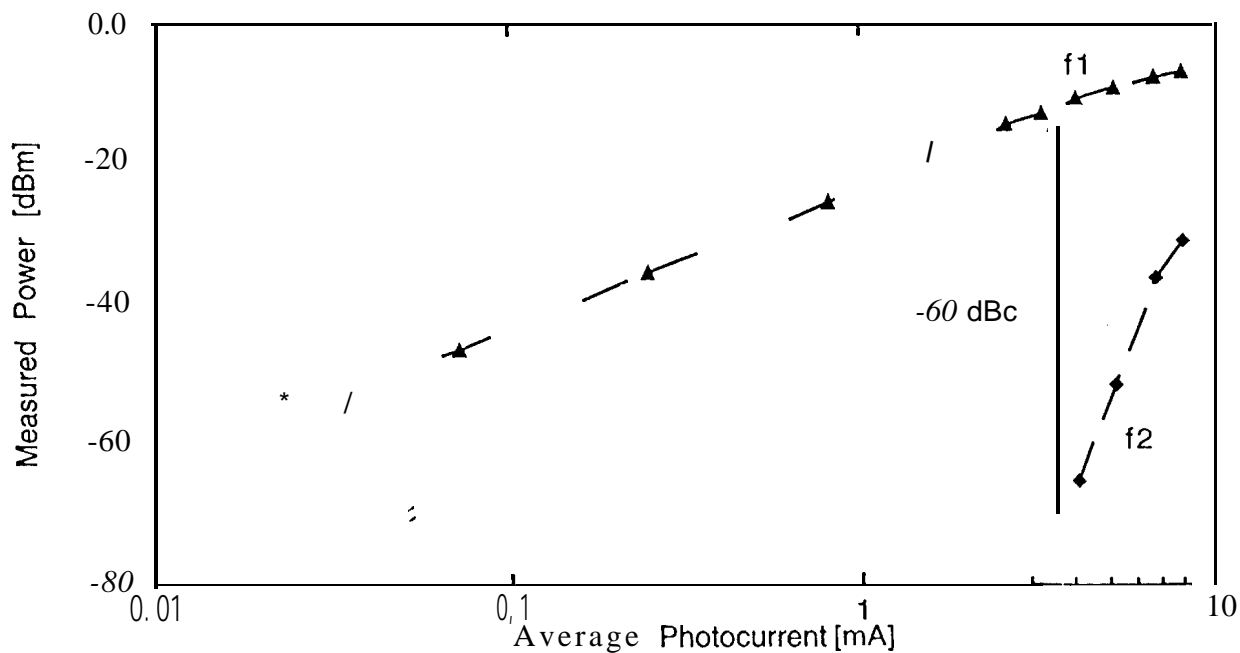


(b)

Fig. 3. Measured photocurrent versus incident power for  $7 \mu\text{m} \times 25 \mu\text{m}$  devices from (a) structure 1 and (b) structure 2 under various reverse biases.

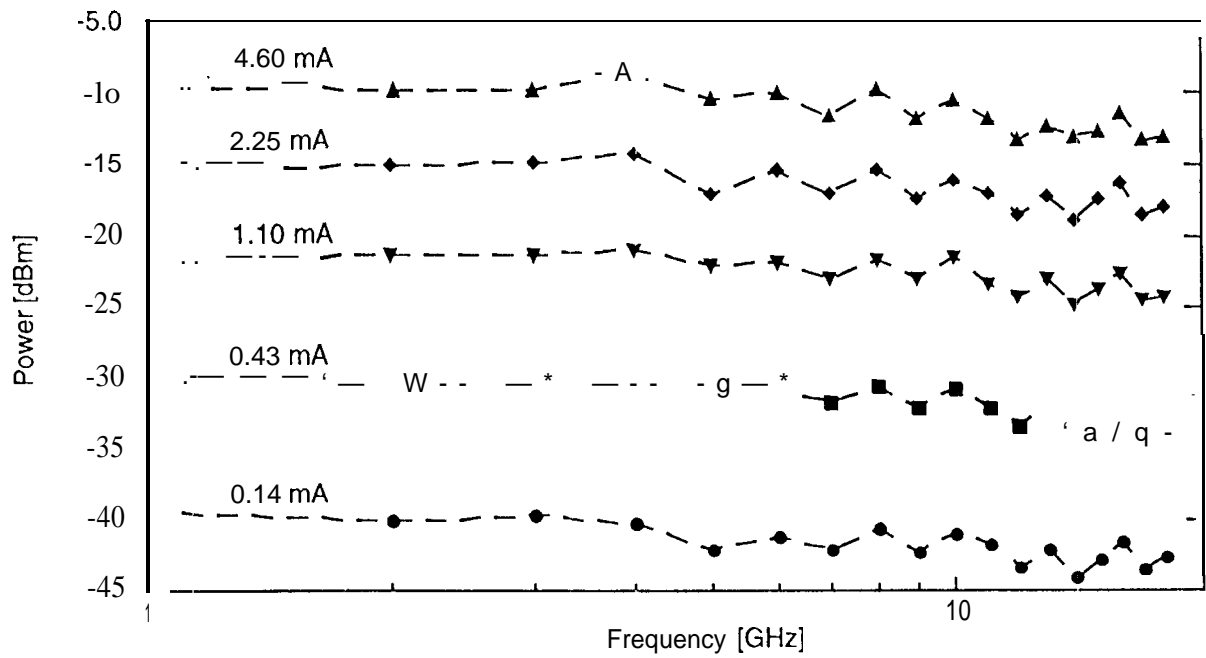


(a)

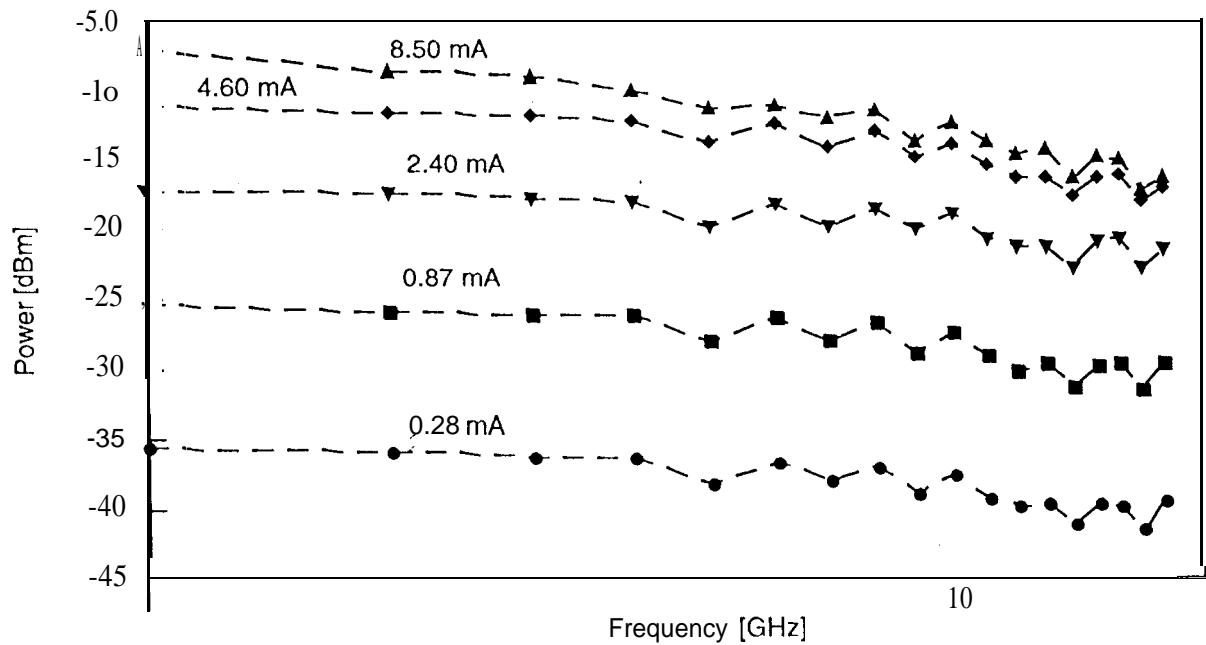


(b)

Fig. 4. The measured harmonic response versus average photocurrent at -3.0 V for  $7\ \mu\text{m} \times 25\ \mu\text{m}$  devices (a) from structure 1 and (b) from structure 2. The -60 dBc photocurrents at -3 V bias are 1.8 mA and 3.5 mA respectively. For this measurement  $f1 = 500\ \text{MHz}$  and  $f2 = 1000\ \text{MHz}$ .



(a)



(b)

Fig. 5. Frequency response of  $7\ \mu\text{m} \times 25\ \text{pm}$  devices from (a) structure 1 biased at  $-6\ \text{V}$  and (b) structure 2 biased at  $-4\ \text{V}$ . The response is measured from  $1\ \text{GHz}$  to  $18\ \text{GHz}$  for various input powers, with the average photocurrent for each input power as indicated.